ACS Photonics

Article

Cite This: ACS Photonics 2018, 5, 844–851

Infrared Plasmonic Resonators Based on Self-Assembled Core–Shell Particles

Kan Yao[†] and Yongmin Liu*[,†,‡]

[†]Department of Electrical and Computer Engineering, Northeastern University, Boston, Massachusetts 02115, United States

[‡]Department of Mechanical and Industrial Engineering, Northeastern University, Boston, Massachusetts 02115, United States

Supporting Information

ABSTRACT: Infrared resonators emerge as key elements of infrared optical devices demanded for widespread applications. Traditional resonators based solely on noble metals suffer from considerable ohmic losses, limited tunability, and low excitation efficiency of surface plasmons in the infrared region, while the alternatives made of high-refractive-index dielectrics encounter fabrication challenges and relatively weak optical coupling. This work presents the experimental demonstration of self-assembled plasmonic core–shell particle clusters exhibiting pronounced and spectrally tunable resonances at infrared, especially mid-infrared, wavelengths. It is shown that the reflection spectra of individual clusters are unique, which are determined by the number and configuration of the constituent particles. Simulation results confirm the measured data and further reveal the origin of the spectral features. These findings pave a new way for the development of complex resonators operating in the infrared region, leading to a substantial step toward reconfigurable plasmonics and metamaterials with potential applications in sensing, imaging, spectroscopy, surveillance, and energy harvesting.

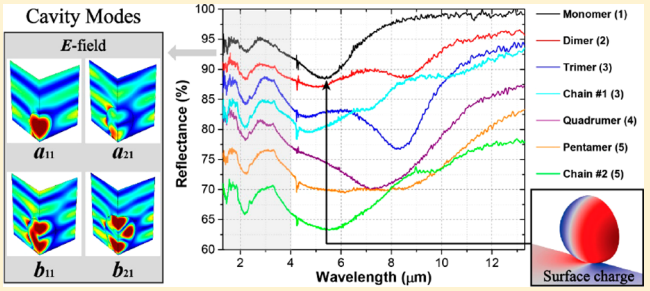

KEYWORDS: *plasmonics, resonators, core–shell particles, self-assembly, infrared spectroscopy*

The use of subwavelength structures to achieve exotic control of electromagnetic fields has stimulated the blossoming of metamaterials and plasmonics over the past decades.[1] In particular, micro- or nanoscale building blocks can resonantly interact with light waves in a predefined manner by programmatically designing their structures and arrangements, which have produced extraordinary properties and innovative photonic devices. Metallic structures play a crucial role in resonators operating in the visible and near-infrared (NIR) region, predominantly because of their capability to support surface plasmons.[2] The collective oscillation of free electrons in metallic structures can couple efficiently with light waves, which ensures strong light–matter interactions required for further construction of metamaterials. However, using metal-based elements as building blocks for metamaterials is accompanied by several limitations, among which the most significant one is the loss. Ohmic losses in metals exist across the entire visible spectrum and remain considerable in the infrared region, while the excitation efficiency of surface plasmons diminishes rapidly as the wavelengths deviate from the visible. Consequently, metals are not ideal platforms for NIR plasmonic devices and are seldom used to implement resonators at mid-infrared (MIR) frequencies.[3,4] On the other hand, infrared optics has found widespread applications in sensing, spectroscopy, biomedical imaging, surveillance, energy harvesting, and so forth.[5] For instance, many biomolecules have their characteristic vibrational and rotational modes located in the infrared region. Sensing devices operating at infrared with high sensitivity are in a pressing need.[6−8]

Recently, high-refractive-index semiconductors such as silicon and germanium are proposed as alternative platforms for infrared metamaterials and photonic devices.[9−13] In addition to their low-loss properties when the photon energy is smaller than the semiconductor band gap, the ease of exciting magnetic resonances and opportunity of tuning the dielectric constants by doping make them very attractive compared with other materials. Nevertheless, there are two main drawbacks of using semiconductors. First, the fabrication is challenging. Although top-down processes are mature techniques to pattern high-index semiconductors, the structures are fixed after fabrication and the feature size is restricted to about 10 nm, which respectively limit the structural tunability and optical coupling strength. Bottom-up approaches such as self-assembly have been demonstrated to achieve metallic colloids with high precision and yield.[14−16] However, for high-index dielectrics, the preparation of regular and uniform micro- or nanoparticles is very difficult. Laser ablation can create small amounts of particles but lacks control of the particle size and roundedness.[12,17−19] Chemically synthesized amorphous silicon particles show improved size uniformity, but they are still far from being identical, hindering the acquisition of strictly symmetric

Received: September 5, 2017
Published: December 7, 2017

DOI: 10.1021/acsphotonics.7b01012
ACS Photonics 2018, 5, 844–851

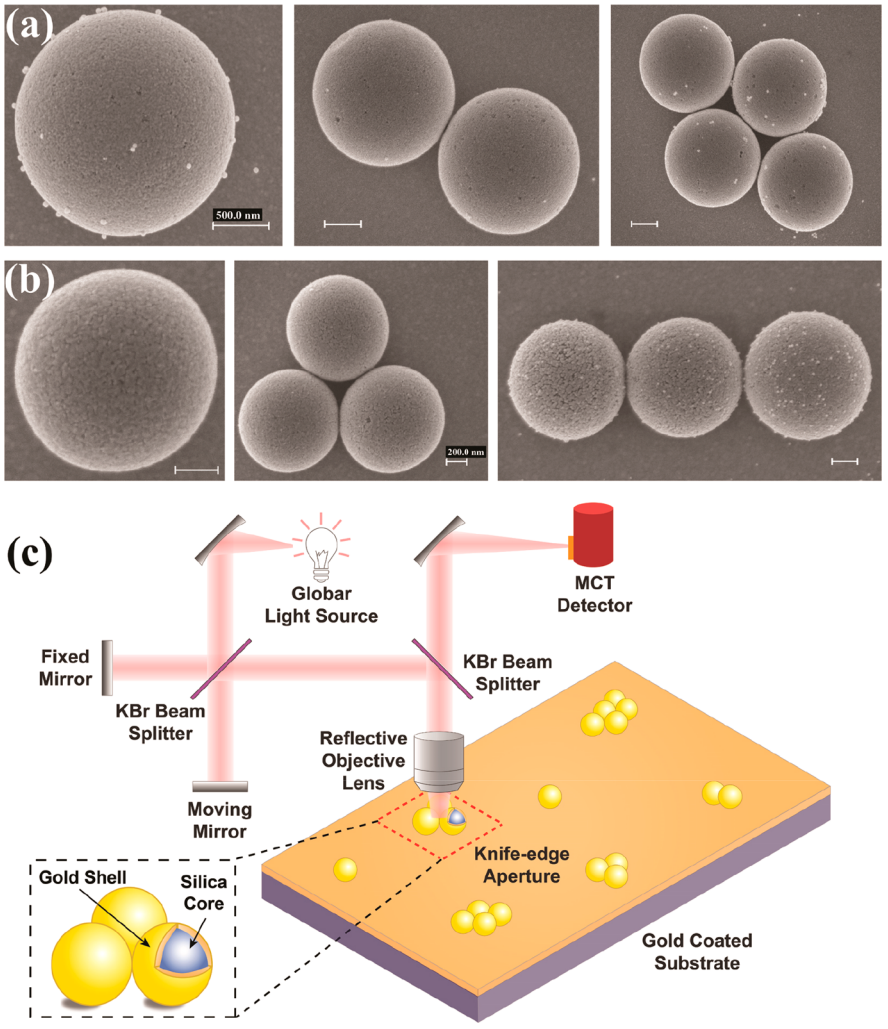

Figure 1. SEM images of representative ensembles consisting of 2 μm (a) and 1 μm (b) core−shell particles on a gold substrate. Scale bars in (a) and (b) are 500 and 200 nm, respectively. (c) Schematic of the FTIR single-particle spectroscopy. The incident infrared light beam is focused by a 36× Cassegrain objective lens on the sample. The reflected light is collected by the same lens and guided to an MCT detector. The rectangle outlined by the red dashed line denotes the knife-edge aperture in FTIR, which allows us to select a single cluster for measurement.

clusters.[11] Second, compared with their metallic counterparts, dielectric particles generate less intense local fields and possess weaker coupling when they are tightly packed.[19,20] The former issue limits the light−matter interaction strength, which is critical in numerous applications such as sensing and spectroscopy; the latter restricts the spectral tunability of the cluster, because introducing additional particles into an existing cluster will not cause significant changes to its optical properties. Therefore, it is an important task to seek suitable building blocks to develop infrared plasmonics and metamaterials with notable spectral tunability.

Core−shell particles consisting of a dielectric core and a metallic shell are a promising solution. Such core−shell particles can support sophisticated, hybridized plasmonic modes as well as cavity modes.[21−26] When they are closely packed into clusters, strong interparticle coupling occurs, giving rise to complex near-field distribution and far-field scattering patterns. With the existence of a reflecting substrate, the interaction becomes even more intriguing.[27−29] In this work, we chemically synthesize and perform self-assembly of SiO_2/Au core−shell particles (SiO_2/Au denotes silica core with gold shell) and systematically characterize their optical properties at the single-cluster level. It is demonstrated that the self-assembled core−shell particles exhibit unique optical properties in the infrared, especially mid-infrared region. Depending on the number and configuration of the constituent particles, the reflection spectra from the individual ensembles show distinct spectral features. In other words, the optical properties of the assembled clusters are sensitive to structural and geometric changes, indicating a promising toolbox for infrared plasmonics, metamaterials, and associated applications. We expect that further improvement could be applied to achieve three-dimensional assemblies and uniform resonator arrays over a larger scale with the assistance of proper stimuli, such as external electric or magnetic fields,[30−32] which would facilitate future realization of reconfigurable plasmonics and metamaterials.

As the starting point, SiO_2/Au core−shell particles were synthesized using a chemical approach reported by Brinson et al. with slight modifications (see Methods).[33−35] The resulting particles consist of a silica core sized 1 or 2 μm and a gold shell of different thicknesses under control. The uniformity of the particle size, roundedness, and surface smoothness ensures that the assembled clusters will be highly symmetric, which in contrast is still challenging for solid metallic and high-index dielectric particles. It is also noted that although Au/SiO_2

DOI: 10.1021/acsphotonics.7b01012
ACS Photonics 2018, 5, 844−851

core−shell particles, usually smaller than 100 nm in diameter, have been extensively studied,[36,37] achieving MIR responses requires large Au core sizes (at least some hundreds of nanometers).[12,38] This is extremely challenging for chemical synthesis and also nonsustainable and cost-ineffective for practical applications. After the synthesis of SiO_2/Au core−shell particles, the self-assembly process was then conducted in a relatively straightforward manner.[24] In brief, a small droplet of the core−shell particle suspension was pipetted on a gold-coated substrate and dried slowly at room temperature. During complete evaporation, the particles were assembled by capillary force randomly into small clusters of different planar geometries. Figure 1a and b show the scanning electron microscope (SEM) images of some representative clusters consisting of 2 and 1 μm particles, respectively. In addition to single particles (monomers), other regular configurations include dimers, trimers, quadrumers, chains of different lengths, and by chance pentamers, heptamers, or larger ensembles (see Figure S1 in the Supporting Information for more images). The interparticle spacing within a cluster was tiny compared with the particle sizes, not larger than 30 nm estimated from the SEM images. On the other hand, the assembled clusters were relatively isolated from each other. The typical distance between neighboring clusters ranged from 10 μm to some hundreds of micrometers. Consequently, the scattering from a cluster will not be affected much by nearby particles, allowing us to characterize the optical properties of individual clusters. From high-magnification SEM images (Figure S2 in the Supporting Information) one can see that the surface smoothness was quite good. Occasionally there were a few cracks, pinhole defects, or excess nanoparticles, which are not avoidable in the synthesis process.[33,34] All these imperfections are much smaller than the particle sizes and wavelengths and hence have negligible influence on the overall optical properties.

Fourier transform infrared (FTIR) spectroscopy was employed to characterize individual clusters with different numbers of core−shell particles and varying configurations. Figure 1c illustrates the schematic of the setup. Detailed description and procedures for the characterization can be found in the Methods section. Uncoated silica beads were first measured as the control experiment. Figure 2a compares the reflection spectra of four different 2 μm clusters on a gold substrate, with the number of constituent silica beads increasing from 1 (monomer) up to 7 (symmetric heptamer). As one can see, in addition to the absorption from CO_2 molecules in air at 4.3 μm and from silica at 8−10 μm, a broad reflection valley appears at 1.5−4 μm, caused mainly by light scattering. However, instead of exhibiting any noticeable shifts, all the spectral features (peaks and dips) line up well in the vertical direction and simply become more evident with the increasing number of particles. This is because the refractive index of silica is relatively low, less than 1.5 below 8 μm. While the particle size is comparable to the wavelengths, no resonance but only limited local field distortion can be induced and the interparticle coupling is weak. This leads to a focusing-like effect at individual particles similar to the photonic jet, which is responsible for the broad reflection dip. The overall scattering from a cluster is simply the summation of those from its constituents. We have performed full-wave simulations of the reflection spectra, which show very good agreement with the experimental results (see Figure S3 in the Supporting Information for simulated spectra and field distributions). It

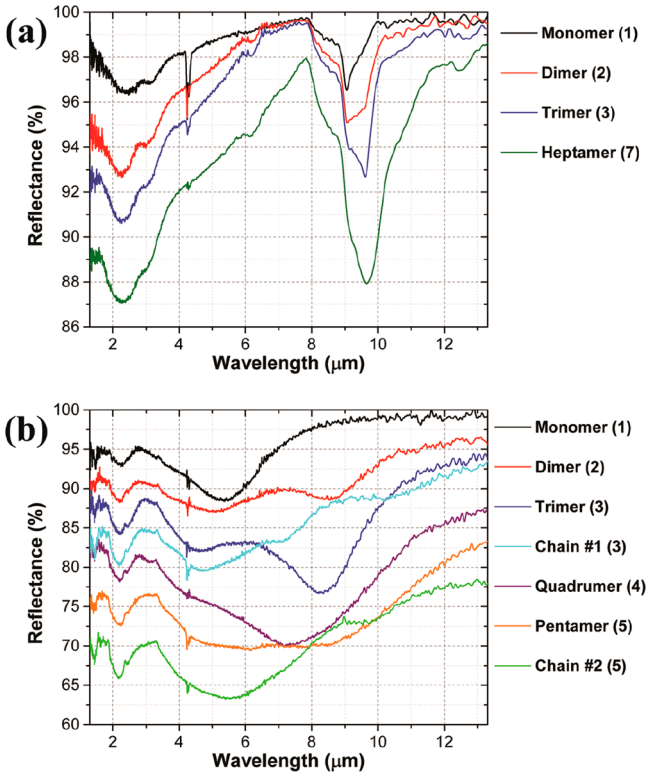

Figure 2. (a) Reflection spectra of uncoated 2 μm silica clusters on a gold substrate. Measured ensembles include a monomer (black), a dimer (red), a symmetric trimer (blue), and a symmetric heptamer (olive). (b) Reflection spectra of 2 μm core−shell SiO_2/Au clusters on a gold substrate. The shell thickness is about 10 nm. Measured ensembles include a monomer (black), a dimer (red), a symmetric trimer (blue), a chain of three (cyan), an asymmetric quadrumer (purple), an asymmetric pentamer (orange), and a chain of five (green). Spectra are shifted vertically for clarity except for the monomer. All the measurements were based on single-cluster FTIR spectroscopy. The numbers given in the figure legend denote the number of particles in each cluster.

should be noted that even for high-index dielectrics the optical properties of a cluster are not strongly dependent on the exact size, number, and aggregation states of the particles, at least when the influence of the substrate is negligible.[19,39] Although a metallic substrate that functions as a mirror is believed to play an important role in modifying the optical response of a single silicon particle,[27,28] experimental studies on reflection from clusters are still lacking, partially because of the challenges in fabricating identical particles for symmetric structures.

The optical property becomes distinctly different for SiO_2/Au core−shell particles. Figure 2b presents the reflection spectra of seven different single clusters in which the particles are coated by a 10 nm gold shell. The gold shell thickness was estimated by SEM at the location of pinhole defects. There are several interesting characteristics in the spectra. First of all, although the sharp dip at 4.3 μm by CO_2 absorption is unavoidable in our experiments, the broad valley at 8−10 μm by SiO_2 absorption disappears. This confirms the high quality of the fabricated core−shells. Any marked cracks or defects on the shell will allow direct illumination on silica, which results in an observable absorption valley in the reflection spectra (Figure S4 in the Supporting Information) and may affect the resonances at shorter wavelengths. Second, compared with the curves in Figure 2a, the reflection from coated particles is

DOI: 10.1021/acsphotonics.7b01012
ACS Photonics 2018, 5, 844−851

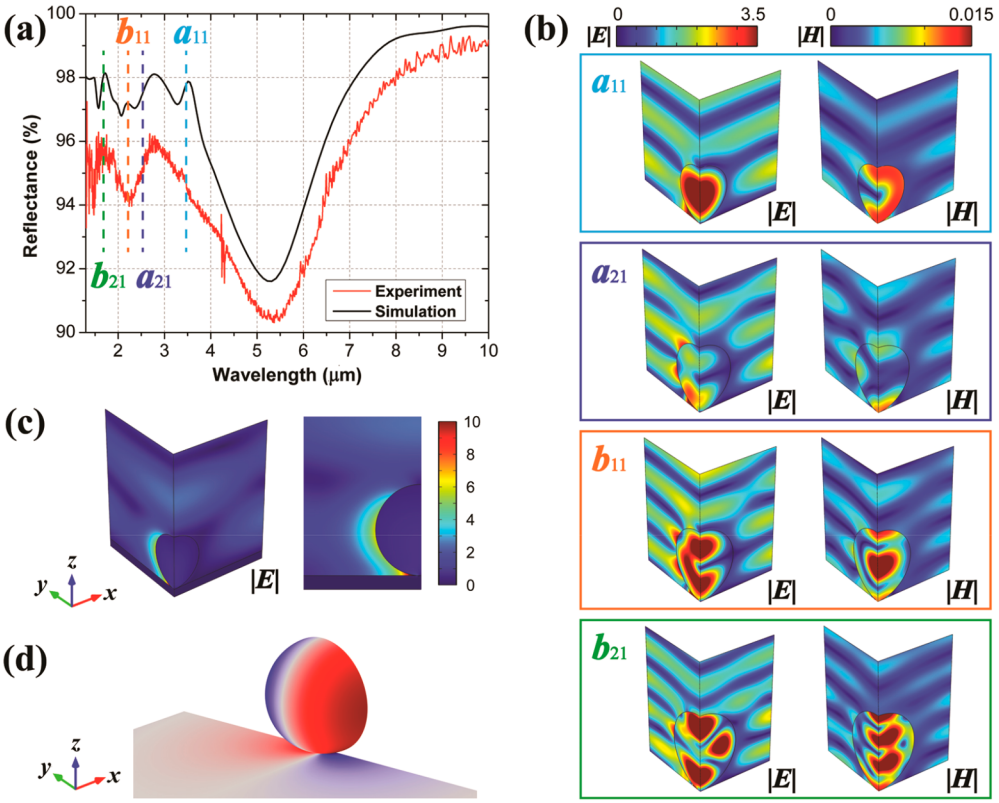

Figure 3. Optical properties of a 2 μm core−shell monomer on a gold substrate. The shell thickness is about 10 nm. (a) Comparison of measured (red) and simulated (black) reflectance. In the simulation, a *y*-polarized plane wave was incident from the top with its electric field amplitude being unity. Representative modes are denoted by the dashed lines. (b) Field intensity maps of the resonant modes and their correspondence to the spectral features. Only one-quarter of the particle is shown because of symmetry. The electric (a_{11}) and magnetic (b_{11}) dipole modes show typical ring-like magnetic and electric field distributions, respectively, whereas the electric (a_{21}) and magnetic (b_{21}) quadrupoles are indicated by the two intensity lobes along the perimeter. (c) Electric field intensity distribution at 5.2 μm. The extremely weak field inside the particle and large field intensity outside the particle in the *y*−*z* plane (right panel) suggest the occurrence of the electric dipole resonance in response to the *y*-polarized incident field. (d) Surface charge density at 5.2 μm wavelength, which also manifests the excitation of the electric dipole resonance of the core−shell particle.

systematically lower, indicating stronger scattering. This is further confirmed by the calculation of extinction cross sections shown in Figure S5 in the Supporting Information. The gold shell either shields the silica core in the long-wavelength region by reflecting most incoming energy directly or forms a cavity in the short-wavelength region by allowing fields to resonate inside and then be re-emitted. Both processes strongly disturb the local field distribution and substantially change the amount of light collected by the detector, leading to complex spectral features. Last but most importantly, each spectrum in Figure 2b shows a unique line shape. The differences are less obvious on the short-wavelength end (<4 μm) due to the close distribution of the fine features but are noticeable in the MIR region. In particular, not only the number of particles, but also their configuration has a role in determining the positions of the spectral minima and maxima. For instance, the spectra of the trimer and the chain of three and of the pentamer and the chain of five show clear differences. Similar phenomena were also observed for clusters consisting of 1 μm core−shell particles in the range of 4−8 μm (Figure S6 in the Supporting Information).

To understand the origin and evolution of the spectral features, we have conduced full-wave simulations using the commercial electromagnetic solver COMSOL Multiphysics. Although Mie theory provides accurate and fast solutions to analyzing the light scattering by spherical particles,[12,40,41] it is difficult to apply the Mie theory in our case with simultaneous occurrence of core−shell structures, complex aggregations, and a reflecting substrate. In our simulations, plane waves at normal incidence were used as the excitation, and the reflectance was calculated from the total extinction cross section of the clusters (see Methods for details). Figure 3a shows the measured and simulated reflectance spectra of a 2 μm core−shell monomer. Very good agreement can be found between the two curves, especially for the peak and dip locations. Moreover, by checking the field distribution at these frequencies, clear correspondence can be established between the spectral features and the resonance modes. Figure 3b plots the mode profiles of four representative multipole resonances, corresponding to the electric dipole (a_{11}), electric quadrupole (a_{21}), magnetic dipole (b_{11}), and magnetic quadrupole (b_{21}), respectively. Here the labeling a_{mn} and b_{mn} follows the convention in Mie theory, with *a* and *b* indicating the electric and magnetic modes, respectively, while the subscripts *m* and *n* accounting for the number of electric field intensity maxima along the circumstantial direction in the hemisphere and along the radial direction.[9] The origin of these modes, noting that all the lobes are well confined in the silica core, is the cavity plasmons.[23,40] Although the refractive index of silica is relatively low and bare cores cannot interact with light resonantly, the metallic shell provides a large refractive index contrast, which helps confine light inside the particles to form good resonators. At certain

DOI: 10.1021/acsphotonics.7b01012
ACS Photonics 2018, 5, 844−851

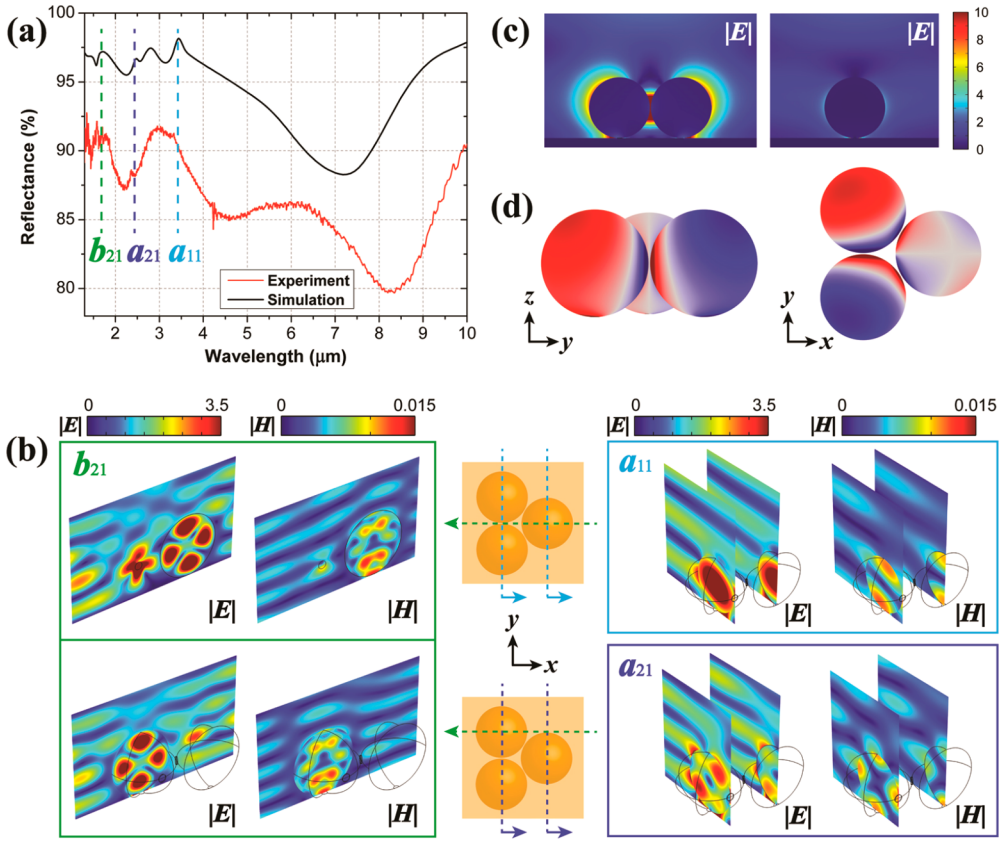

Figure 4. Optical properties of a 2 μm core−shell trimer on a gold substrate. The shell thickness is about 10 nm. (a) Comparison of measured (red) and simulated (black) reflectance. In the simulation, a *y*-polarized plane wave was incident from the top. Representative modes are marked by the dashed lines. (b) Field intensity maps of the resonant modes and their correspondence to the spectral features. The colored dashed lines in the central panels indicate the position of the cutting planes for observing different mode profiles. Only half of the trimer is shown because of symmetry. Compared with Figure 3, the electric dipole (a_{11}) and magnetic quadrupole (b_{21}) are still conspicuous and almost unshifted. The electric quadrupole (a_{21}) becomes visible due to the interparticle coupling, while the magnetic dipole (b_{11}) diminishes. (c) Electric field distribution at 7 μm wavelength. The intense field in the gap between two particles (left panel) suggests strong coupling between the electric dipole modes of the two particles. In contrast, the third particle (right panel) is off-resonance. (d) Surface charge density at 7 μm seen from the dimer side (left panel) and from the top (right panel). Both confirm the strong dipole resonances in the dimer.

frequencies, optical fields that enter the cavity circulate along the perimeter and constructively interfere with themselves after each cycle.[23] This is especially clear for high-order resonances. From the field intensity maps, one can see that the a_{11}, b_{11}, and b_{21} modes are quite strong compared with the field outside the particle. Hence they are more pronounced in the spectrum. The mode a_{21}, in contrast, is much weaker and can hardly affect the scattering in the far field. In our experiments, the b_{11} feature was not clearly observable in the spectra of the monomer, partially because of the relatively strong noise. With increasing number of particles and proper aggregation states, b_{11} may appear, such as in the chain of three (cyan curve in Figure 2b and Figure S7 in the Supporting Information). Higher order modes also exist at shorter wavelengths (Figure S8 in the Supporting Information), while they are not the main focus of this work. The optical cavity modes in core−shell particles may offer unique avenues to lasing, photovoltaic, and sensing applications. With a dye-doped dielectric core, individual core−shell particles can be used for plasmonic laser or spaser generation.[42,43] By sculpting the gold shell (via etching or milling), it is even possible to control the direction of laser/spaser emission.[44] In addition, integrated with upconversion materials, the core−shell particles can increase the upconversion efficiency for solar energy harvesting by enhancing either the excitation strength or the emission strength.[45] The abundant and widespread fine spectral features from cavity modes are also useful for simultaneously detecting distinct analytes with different infrared fingerprints. Adsorption of target molecules on the gold shell could induce measurable changes in the position and amplitude of the resonances.[46] In these applications, the mechanism is distinctly different from the platforms based on metallic core/dielectric shell nanoparticles, where signal enhancement results from the resonance of the metallic core, while the dielectric shell functions as spacers and binding sites of molecules.

The most evident feature in Figure 3a is the deep valley centered at ~5.2 μm. The field intensity map in Figure 3c reveals that it does not correspond to any plasmonic cavity modes inside the particle. At longer wavelengths, even the 10 nm shell thickness is already comparable with the penetration depth of gold. Therefore, instead of forming a cavity, the shell interacts with light more like a solid gold particle (Figure S9 in the Supporting Information), and the broad reflection valley corresponds to the fundamental electric dipole resonance of the particle, as indicated by the field intensity map in Figure 3c and the surface charge density in Figure 3d. This also means that we do not need Au/SiO_2 core−shell particles with a large Au core to achieve the pronounced MIR resonance. The in-plane dipole

DOI: 10.1021/acsphotonics.7b01012
ACS Photonics 2018, 5, 844−851

moment is broadband and scatters light strongly in the plane perpendicular to its own orientation, and only a small portion of the energy can be collected by the detector on the top. In addition, because the particle sits on a gold substrate, a mirror-image dipole can be excited, which further enhances the scattering.[27] Consequently, a broad reflection valley occurs. In contrast, for the same particle in free space or on a low-index substrate, although more cavity modes can be excited, the scattering at the fundamental electric dipole resonance is much weaker (Figure S10 in the Supporting Information). Therefore, the modification of the optical properties of particles by a substrate is significant, and from a practical point of view, this allows effective tuning of the resonances of given particles.[47] From Figure 3c, it can also be seen that the local field at the bottom of the particle is extremely intense because of the vanishing gap size. This hot spot could be used in surface-enhanced infrared absorption spectroscopy and cavity-enhanced single-molecule coupling for various applications at MIR frequencies.[6,48,49]

It is also worth investigating how the aggregation of particles will change the optical properties. Figure 4a plots the measured and simulated reflectance spectra from a 2 μm trimer. At normal incidence, its optical response is nearly isotropic and insensitive to the polarization.[50] The two curves again agree with each other very well for wavelengths shorter than 5 μm, where the resonance modes and spectral features show nice correspondence. Compared with the spectra of a monomer in Figure 3, interestingly, the interparticle coupling in a cluster induces clear changes in the spectrum and the associated mode profiles. The electric dipole mode (a_{11}) and magnetic quadrupole mode (b_{21}) do not change much in position, and the dipole peak is slightly broadened. Both modes are excited almost equally in the three particles as in the monomer case. Therefore, these two peaks appear more evident due to stronger signals from the increased number of particles. In contrast, the magnetic dipole (b_{11}) is still difficult to recognize in the spectrum. From the field distribution (data not shown), it is found that the magnetic dipole mode cannot be excited efficiently in the two particles forming a dimer, likely because the shell is not thick enough to isolate the two particles as two individual resonators. The electric quadrupole mode (a_{21}), nearly invisible in the spectrum of a monomer, starts to emerge in the trimer case. From the field distributions in Figure 4b, although the internal field intensities in the dimer and in the monomer are not equal, they are both stronger than that of the external field and, thus, capable of disturbing the scattering patterns and evident in the spectrum.

Provided the cavity modes are largely confined inside the core−shell particles, the spectral changes from interparticle coupling or mode hybridization is not very significant at short wavelengths. On the other hand, the fundamental dipole resonances of the particles, owing to the large mode volume, can interact with each other and greatly modify the spectra in the MIR region. By comparing the curves in Figures 3a and 4a, it is apparent that the main dip of reflection is shifted from ∼5.2 μm to ∼8.3 μm when the particles are assembled into a trimer. The discrepancy between simulation and measurement in Figure 4a is probably caused by the simplified modeling of the normal incidence. At the major reflection dip, one can see from Figure 4c that intense fields from the dipole resonances are excited on the dimer side (left panel), while the adjacent monomer appears off-resonance (right panel). Moreover, the surface charge density shown in Figure 4d clearly reveals that the electric dipoles in the dimer are parallel, which are superradiant, leading to the major reflection minimum. For other geometries, the MIR optical properties are polarization-dependent. In general, aggregation of particles along the polarization direction leads to red-shifted resonances[24] and complex distributions of hot spots at the interparticle gaps and particle−substrate gaps.[29] As an example, a brief analysis on the chain of three is presented in Figure S11 in the Supporting Information, which shows qualitative agreement with the experimental data. However, further identification of the polarization-dependent features at the single-cluster level is limited by the brightness of the light source and the sensitivity of the detector. The configuration of the cluster determines in a unique way how the dipole modes from each constituent particle interplay with each other. Consequently, the reflectance spectra in the mid-infrared region become highly tunable, as shown in Figure 2b. It should be noted that the results presented in this work are all based on unpolarized light at near-normal incidence. We predict that with polarized illumination the observation of not only conventional polarization-dependent features but also some exotic topological states is possible.[51] Furthermore, introduction of light at large incident angles could excite more complicated features, such as the magnetic resonance in trimers and Fano resonances in larger clusters.[24,25]

In summary, we report the experimental demonstration of self-assembled plasmonic core−shell particle clusters for infrared resonators. High-quality core−shell SiO_2/Au particles were synthesized using chemical approaches, which enables assembly of highly symmetric clusters. Depending on the number and configuration of the constituent particles, the reflection spectra from single ensembles are unique. The optical properties of the assembled clusters are very sensitive to structural and geometric changes. By comparing the FTIR single-cluster spectra with simulation results, plasmonic cavity multipole resonances were identified for spectral features between 1.3 and 4 μm. Moreover, we show that the complex interplay between the dipole modes of each core−shell particle gives rise to distinct line shapes in the long-wavelength range (4−10 μm). These results manifest the use of plasmonic core−shell particles as a promising toolbox for infrared resonators and associated applications, such as sensing, imaging, spectroscopy, and energy harvesting. We expect that further improvement could be applied to achieve three-dimensional structures and uniform resonator arrays over a larger scale, paving an avenue toward future realization of reconfigurable plasmonics and metamaterials.

METHODS

Synthesis of Core−Shell SiO_2/Au Particles. We followed the protocol reported by Brinson et al. to synthesize core−shell SiO_2/Au particles.[33] In brief, as-purchased plain silica beads (1 and 2 μm) were washed carefully and dispersed in ethanol at a proper concentration. 3-Aminopropyltriethoxysilane (APTES) was used to modify the surface of the beads. Gold nanoparticles of 1−2 nm were prepared according to Duff et al. and attached to the modified silica beads, serving as seeds or nucleation sites for later shell formation. After mixing the resulting particles with aged chloroauric acid planting solution (mixed with potassium carbonate), subsequent reduction of gold ions was conducted by adding a certain amount of formaldehyde. The attached gold nanoparticles first increased in size and then began to coalesce on the surface of the silica cores, eventually

DOI: 10.1021/acsphotonics.7b01012
ACS Photonics 2018, 5, 844−851

forming a complete gold shell. Typical shell thicknesses ranged from 10 to 15 nm for 2 μm particles depending on the gold ion to silica bead ratios, which were measured at the edges of a surface cut made by ion beams (Figure S12 in the Supporting Information). The surface roughness, apart from occasional cracks, pinhole defects, and attachments of excess nanoparticles, was sub-5 nm estimated from SEM images (Figure S2 in the Supporting Information). The synthesized core−shell particles were washed immediately for storage and self-assembly.

Bright-Field Reflection FTIR Measurements. FTIR measurements were performed using a Bruker Vertex 70 spectrometer combined with a Hyperion 1000 microscope. The IR light was generated by a globar source and then focused on the sample surface by a 36× Cassegrain objective (NA = 0.5), which shapes the incident light beam to be half of an annulus in cross section, corresponding to incident angles ranging from ∼18° to 30°. Reflected light was collected by the same objective and guided to a mercury−cadmium−telluride (MCT) detector. In order to measure the reflection from a single ensemble, a knife-edge aperture in the conjugate image plane was carefully adjusted to define a rectangular area that contained exclusively the cluster of interest. Depending on the signal-to-noise ratio (SNR) as well as the number and configuration of the particles in the clusters, the size and shape of the aperture varied, roughly from 100 to 400 μm^2. Focusing was carefully tuned to maximize the signal intensity. For each measurement, the sample was scanned at least 2500 times with a 4 cm^{-1} spectral resolution and a proper amplification. This scheme can effectively suppress undesired noise and increase SNR. The reference measurement in a sample-free area was carried out immediately after each sample measurement, while all the settings including focusing, knife-edge aperture size, scan times, and resolution must remain unchanged. Reflectance was then calculated by normalizing the sample spectrum to the reference spectrum. All measurements were based on unpolarized illumination.

Simulations. Finite element method (FEM) modeling was done by using the COMSOL Multiphysics 4.4 RF module. The scattering (reflection) spectra of different clusters on a gold substrate were calculated. In the simulations, the incident light was launched from the top as a linearly polarized plane wave, and the reflectance R was obtained from the extinction cross section σ_{ext} via the formula $R = 1 - \sigma_{ext}/A$. Here A is a constant corresponding to the knife-edge aperture size. Although the equation and the above settings do not fully reflect the real configurations used in the experiments, which prevents perfect match between the simulated and measured spectra, they serve as a very good approximation that captures the right physics and manifests most spectral features.[9,27] When applicable, symmetry planes were used to reduce the size of the simulation domain. The interparticle spacing was chosen as 20 nm. Smaller gaps will not cause noticeable changes in the spectra but lead to heavier meshing loads. Considering the very large core−shell aspect ratios, the particles were modeled as solid silica spheres with transition boundary conditions (TBCs), which mimic gold shells of finite thicknesses. The validity of this simplification was confirmed by comparing the reflection from a 2 μm trimer with TBCs and that from a trimer of the same cores but coated by a uniform 50 nm gold shell. The results showed quantitatively excellent agreement throughout the frequency range of interest. The permittivity of gold was taken from the Rakić data,[52] and the refractive index of silica was from Kischkat et al.[53]

■ ASSOCIATED CONTENT

Supporting Information

The Supporting Information is available free of charge on the ACS Publications website at DOI: 10.1021/acsphotonics.7b01012.

Additional information (PDF)

■ AUTHOR INFORMATION

Corresponding Author

*E-mail: y.liu@northeastern.edu.

ORCID

Yongmin Liu: 0000-0003-1084-6651

Notes

The authors declare no competing financial interest.

■ ACKNOWLEDGMENTS

We thank Liao Chen and Anna Nardella for assistance with chemical synthesis. We acknowledge the financial support from the Office of Naval Research (N00014-16-1-2409) and the technical and instrumental support from the George J. Kostas Nanoscale Technology and Manufacturing Research Center at Northeastern University.

■ REFERENCES

(1) Yao, K.; Liu, Y. Plasmonic Metamaterials. *Nanotechnol. Rev.* **2014**, *3*, 177−210.

(2) Barnes, W. L.; Dereux, A.; Ebbesen, T. W. Surface Plasmon Subwavelength Optics. *Nature* **2003**, *424*, 824−830.

(3) Naik, G. V.; Shalaev, V. M.; Boltasseva, A. Alternative Plasmonic Materials: Beyond Gold and Silver. *Adv. Mater.* **2013**, *25*, 3264−3294.

(4) Zhong, Y.; Malagari, S. D.; Hamilton, T.; Wasserman, D. Review of Mid-Infrared Plasmonic Materials. *J. Nanophotonics* **2015**, *9*, 093791.

(5) Law, S.; Podolskiy, V.; Wasserman, D. Towards Nano-Scale Photonics with Micro-Scale Photons: the Opportunities and Challenges of Mid-Infrared Plasmonics. *Nanophotonics* **2013**, *2*, 103−130.

(6) Rodrigo, D.; Limaj, O.; Janner, D.; Etezadi, D.; de Abajo, F. J. G.; Pruneri, V.; Altug, H. Mid-Infrared Plasmonic Biosensing with Graphene. *Science* **2015**, *349*, 165−168.

(7) Wu, C.; Khanikaev, A. B.; Adato, R.; Arju, N.; Yanik, A. A.; Altug, H.; Shvets, G. Fano-Resonant Asymmetric Metamaterials for Ultrasensitive Spectroscopy and Identification of Molecular Monolayers. *Nat. Mater.* **2012**, *11*, 69−75.

(8) Zeng, S.; Sreekanth, K. V.; Shang, J.; Yu, T.; Chen, C.-K.; Yin, F.; Baillargeat, D.; Coquet, P.; Ho, H.-P.; Kabashin, A. V.; Yong, K.-T. Graphene−Gold Metasurface Architectures for Ultrasensitive Plasmonic Biosensing. *Adv. Mater.* **2015**, *27*, 6163−6169.

(9) Fenollosa, R.; Meseguer, F.; Tymczenko, M. Silicon Colloids: from Microcavities to Photonic Sponges. *Adv. Mater.* **2008**, *20*, 95−98.

(10) Shi, L.; Tuzer, T. U.; Fenollosa, R.; Meseguer, F. A New Dielectric Metamaterial Building Block with a Strong Magnetic Response in the Sub-1.5-Micrometer Region: Silicon Colloid Nanocavities. *Adv. Mater.* **2012**, *24*, 5934−5938.

(11) Shi, L.; Harris, J. T.; Fenollosa, R.; Rodriguez, I.; Lu, X.; Korgel, B. A.; Meseguer, F. Monodisperse Silicon Nanocavities and Photonic Crystals with Magnetic Response in the Optical Region. *Nat. Commun.* **2013**, *4*, 1904.

(12) Lewi, T.; Iyer, P. P.; Butakov, N. A.; Mikhailovsky, A. A.; Schuller, J. A. Widely Tunable Infrared Antennas Using Free Carrier Refraction. *Nano Lett.* **2015**, *15*, 8188−8193.

(13) Jahani, S.; Jacob, Z. All-Dielectric Metamaterials. *Nat. Nanotechnol.* **2016**, *11*, 23−36.

DOI: 10.1021/acsphotonics.7b01012
ACS Photonics 2018, 5, 844−851

(14) Lee, J. H.; Wu, Q.; Park, W. Metal Nanocluster Metamaterial Fabricated by the Colloidal Self-Assembly. *Opt. Lett.* **2009**, *34*, 443−445.
(15) Henzie, J.; Grünwald, M.; Widmer-Cooper, A.; Geissler, P. L.; Yang, P. Self-Assembly of Uniform Polyhedral Silver Nanocrystals into Densest Packings and Exotic Superlattices. *Nat. Mater.* **2012**, *11*, 131−137.
(16) Mühlig, S.; Cunningham, A.; Dintinger, J.; Scharf, T.; Bürgi, T.; Lederer, F.; Rockstuhl, C. Self-Assembled Plasmonic Metamaterials. *Nanophotonics* **2013**, *2*, 211−240.
(17) Evlyukhin, A. B.; Novikov, S. M.; Zywietz, U.; Eriksen, R. L.; Reinhardt, C.; Bozhevolnyi, S. I.; Chichkov, B. N. Demonstration of Magnetic Dipole Resonances of Dielectric Nanospheres in the Visible Region. *Nano Lett.* **2012**, *12*, 3749−3755.
(18) Fu, Y. H.; Kuznetsov, A. I.; Miroshnichenko, A. E.; Yu, Y. F.; Luk'yanchuk, B. Directional Visible Light Scattering by Silicon Nanoparticles. *Nat. Commun.* **2013**, *4*, 1527.
(19) Yan, J. H.; Liu, P.; Lin, Z. Y.; Wang, H.; Chen, H. J.; Wang, C. X.; Yang, G. W. Magnetically Induced Forward Scattering at Visible Wavelengths in Silicon Nanosphere Oligomers. *Nat. Commun.* **2015**, *6*, 7042.
(20) Bakker, R. M.; Permyakov, D.; Yu, Y. F.; Markovich, D.; Paniagua-Domínguez, R.; Gonzaga, L.; Samusev, A.; Kivshar, Y.; Luk'yanchuk, B.; Kuznetsov, A. I. Magnetic and Electric Hotspots with Silicon Nanodimers. *Nano Lett.* **2015**, *15*, 2137−2142.
(21) Prodan, E.; Radloff, C.; Halas, N. J.; Nordlander, P. A Hybridization Model for the Plasmon Response of Complex Nanostructures. *Science* **2003**, *302*, 419−422.
(22) Knight, M. W.; Halas, N. J. Nanoshells to Nanoeggs to Nanocups: Optical Properties of Reduced Symmetry Core-Shell Nanoparticles beyond the Quasistatic Limit. *New J. Phys.* **2008**, *10*, 105006.
(23) Penninkhof, J. J.; Sweatlock, L. A.; Moroz, A.; Atwater, H. A.; van Blaaderen, A.; Polman, A. Optical Cavity Modes in Gold Shell Colloids. *J. Appl. Phys.* **2008**, *103*, 123105.
(24) Fan, J. A.; Wu, C.; Bao, K.; Bao, J.; Bardhan, R.; Halas, N. J.; Manoharan, V. N.; Nordlander, P.; Shvets, G.; Capasso, F. Self-Assembled Plasmonic Nanoparticle Clusters. *Science* **2010**, *328*, 1135−1138.
(25) Fan, J. A.; Bao, K.; Wu, C.; Bao, J.; Bardhan, R.; Halas, N. J.; Manoharan, V. N.; Shvets, G.; Nordlander, P.; Capasso, F. Fano-Like Interference in Self-Assembled Plasmonic Quadrumer Clusters. *Nano Lett.* **2010**, *10*, 4680−4685.
(26) Sheikholeslami, S. N.; Alaeian, H.; Koh, A. L.; Dionne, J. A. A Metafluid Exhibiting Strong Optical Magnetism. *Nano Lett.* **2013**, *13*, 4137−4141.
(27) Xifré-Pérez, E.; Shi, L.; Tuzer, U.; Fenollosa, R.; Ramiro-Manzano, F.; Quidant, R.; Meseguer, F. Mirror-Image-Induced Magnetic Modes. *ACS Nano* **2013**, *7*, 664−668.
(28) Miroshnichenko, A. E.; Evlyukhin, A. B.; Kivshar, Y. S.; Chichkov, B. N. Substrate-Induced Resonant Magnetoelectric Effects for Dielectric Nanoparticles. *ACS Photonics* **2015**, *2*, 1423−1428.
(29) Chen, S.; Meng, L. Y.; Shan, H. Y.; Li, J. F.; Qian, L.; Williams, T.; Yang, Z.-L.; Tian, Z.-Q. How to Light Special Hot Spots in Multiparticle−Film Configurations. *ACS Nano* **2016**, *10*, 581−587.
(30) Ma, F.; Wang, S.; Wu, D. T.; Wu, N. Electric-Field−Induced Assembly and Propulsion of Chiral Colloidal Clusters. *Proc. Natl. Acad. Sci. U. S. A.* **2015**, *112*, 6307−6312.
(31) Erb, R. M.; Son, H. S.; Samanta, B.; Rotello, V. M.; Yellen, B. B. Magnetic Assembly of Colloidal Superstructures with Multipole Symmetry. *Nature* **2009**, *457*, 999−1002.
(32) Zhang, M.; Magagnosc, D. J.; Liberal, I.; Yu, Y.; Yun, H.; Yang, H.; Wu, Y.; Guo, J.; Chen, W.; Shin, Y. J.; Stein, A.; Kikkawa, J. M.; Engheta, N.; Gianola, D. S.; Murray, C. B.; Kagan, C. R. High-Strength Magnetically Switchable Plasmonic Nanorods Assembled from a Binary Nanocrystal Mixture. *Nat. Nanotechnol.* **2016**, *12*, 228−233.
(33) Brinson, B. E.; Lassiter, J. B.; Levin, C. S.; Bardhan, R.; Mirin, N.; Halas, N. J. Nanoshells Made Easy: Improving Au Layer Growth on Nanoparticle Surfaces. *Langmuir* **2008**, *24*, 14166−14171.
(34) Graf, C.; van Blaaderen, A. Metallodielectric Colloidal Core-Shell Particles for Photonic Applications. *Langmuir* **2002**, *18*, 524−534.
(35) Oldenburg, S. J.; Averitt, R. D.; Westcott, S. L.; Halas, N. J. Nanoengineering of Optical Resonances. *Chem. Phys. Lett.* **1998**, *288*, 243−247.
(36) Liz-Marzán, L. M.; Giersig, M.; Mulvaney, P. Synthesis of Nanosized Gold-Silica Core-Shell Particles. *Langmuir* **1996**, *12*, 4329−4335.
(37) Lu, Y.; Yin, Y.; Li, Z.-Y.; Xia, Y. Synthesis and Self-Assembly of Au@SiO_2 Core-Shell Colloids. *Nano Lett.* **2002**, *2*, 785−788.
(38) Lauri, A.; Velleman, L.; Xiao, X.; Cortés, E.; Edel, J. B.; Giannini, V.; Rakovich, A.; Maier, S. A. 3D Conforcal Raman Tomography to Probe Field Enhancements inside Supercluster Metamaterials. *ACS Photonics* **2017**, *4*, 2070−2077.
(39) Xifré-Pérez, E.; de Abajo, F. G.; Fenollosa, R.; Meseguer, F. Photonic Binding in Silicon-Colloid Microcavities. *Phys. Rev. Lett.* **2009**, *103*, 103902.
(40) Gu, P.; Wan, M.; Shen, Q.; He, X.; Chen, Z.; Zhan, P.; Wang, Z. Experimental Observation of Sharp Cavity Plasmon Resonances in Dielectric-Metal Core-Shell Resonators. *Appl. Phys. Lett.* **2015**, *107*, 141908.
(41) Bohren, C. F.; Huffman, D. R. *Absorption and Scattering of Light by Small Particles*; John Wiley & Sons, 2008.
(42) Stockman, M. I. Spasers Explained. *Nat. Photonics* **2008**, *2*, 327−329.
(43) Noginov, M. A.; Zhu, G.; Belgrave, A. M.; Bakker, R.; Shalaev, V. M.; Narimanov, E. E.; Stout, S.; Herz, E.; Suteewong, T.; Wiesner, U. Demonstration of A Spaser-Based Nanolaser. *Nature* **2009**, *460*, 1110−1112.
(44) Meng, X.; Guler, U.; Kildishev, A. V.; Fujita, K.; Tanaka, K.; Shalaev, V. M. Unidirectional Spaser in Symmetry-Broken Plasmonic Core-Shell Nanocavity. *Sci. Rep.* **2013**, *3*, 1241.
(45) de Wild, J.; Meijerink, A.; Rath, J. K.; van Sark, W. G. J. H. M.; Schropp, R. E. I. Upconverter Solar Cells: Materials and Applications. *Energy Environ. Sci.* **2011**, *4*, 4835−4848.
(46) Raschke, G.; Brogl, S.; Susha, A. S.; Rogach, A. L.; Klar, T. A.; Feldmann, J. Gold Nanoshells Improve Single Nanoparticle Molecular Sensors. *Nano Lett.* **2004**, *4*, 1853−1857.
(47) Sobhani, A.; Manjavacas, A.; Cao, Y.; McClain, M. J.; de Abajo, F. J. G.; Nordlander, P.; Halas, N. J. Pronounced Linewidth Narrowing of an Aluminum Nanoparticle Plasmon Resonance by Interaction with an Aluminum Metallic Film. *Nano Lett.* **2015**, *15*, 6946−6951.
(48) Chikkaraddy, R.; de Nijs, B.; Benz, F.; Barrow, S. J.; Scherman, O. A.; Rosta, E.; Demetriadou, A.; Fox, P.; Hess, O.; Baumberg, J. J. Single-Molecule Strong Coupling at Room Temperature in Plasmonic Nanocavities. *Nature* **2016**, *535*, 127−130.
(49) Li, M.; Cushing, S. K.; Wu, N. Plasmon-Enhanced Optical Sensors: a Review. *Analyst* **2015**, *140*, 386−406.
(50) Chuntonov, L.; Haran, G. Trimeric Plasmonic Molecules: the Role of Symmetry. *Nano Lett.* **2011**, *11*, 2440−2445.
(51) Poddubny, A.; Miroshnichenko, A.; Slobozhanyuk, A.; Kivshar, Y. Topological Majorana States in Zigzag Chains of Plasmonic Nanoparticles. *ACS Photonics* **2014**, *1*, 101−105.
(52) Rakić, A. D.; Djurišić, A. B.; Elazar, J. M.; Majewski, M. L. Optical Properties of Metallic Films for Vertical-Cavity Optoelectronic Devices. *Appl. Opt.* **1998**, *37*, 5271−5283.
(53) Kischkat, J.; Peters, S.; Gruska, B.; Semtsiv, M.; Chashnikova, M.; Klinkmüller, M.; Fedosenko, O.; Machulik, S.; Aleksandrova, A.; Monastyrskyi, G.; Flores, Y.; Masselink, W. T. Mid-Infrared Optical Properties of Thin Films of Aluminum Oxide, Titanium Dioxide, Silicon Dioxide, Aluminum Nitride, and Silicon Nitride. *Appl. Opt.* **2012**, *51*, 6789−6798.

DOI: 10.1021/acsphotonics.7b01012
ACS Photonics 2018, 5, 844−851